Available online at www.sciencedirect.com
SCIENCE DIRECT®
Acta Materialia 53 (2005) 3469–3477
Acta MATERIALIA
www.actamat-journals.com

Mechanical behavior of shear bands and the effect of their relaxation in a rolled amorphous Al-based alloy

W.H. Jiang [a], F.E. Pinkerton [b], M. Atzmon [a,c,*]

[a] Department of Nuclear Engineering and Radiological Sciences, University of Michigan, Cooley Laboratory, North Campus, Ann Arbor, MI 48109-2104, USA
[b] General Motors R&D Center, 30500 Mound Road, Warren, MI 48090, USA
[c] Department of Materials Science and Engineering, University of Michigan, Ann Arbor, MI 48109-2104, USA

Received 3 February 2005; received in revised form 31 March 2005; accepted 4 April 2005
Available online 12 May 2005

Abstract

Using nanoindentation, atomic force microscopy and high-resolution transmission electron microscopy (HRTEM), the effect of cold rolling and subsequent annealing on the microstructure and mechanical behavior of an amorphous Al–Ni–Y alloy has been investigated. Rolling moderates the serrated flow as compared with the as-spun alloy. Annealing recovers the serrated flow, and the rolled/annealed sample exhibits even more pronounced serrations than the as-spun sample. Rolling reduces the hardness, whereas annealing enhances it substantially. Combining HRTEM with frequency filtering, nanovoids at shear bands in the rolled and rolled/annealed samples were imaged. In the rolled sample, a great number of nanovoids are located in the interior of shear bands. Annealing does not change their distribution. The excess free volume has a more substantial impact on the plastic-deformation resistance of shear bands than do the nanovoids.

Keywords: Amorphous alloys; Plastic deformation; Annealing; High-resolution electron microscopy; Shear bands

1. Introduction

Plastic deformation of amorphous alloys at low homologous temperatures and high strain rates is characterized by inhomogeneity and is concentrated in highly localized, narrow, deformation regions, i.e., shear bands. Shear bands are a microstructural feature unique to deformed amorphous alloys, resulting, e.g., from bending [1–5], compression [6], tension [7] and nanoindentation [8–10]. Excessive propagation of individual shear bands may cause premature fracture [11,12]. Undoubtedly, the formation of shear bands severely limits its mechanical processing and applications of amorphous alloys.

Several approaches have been taken to overcome the deleterious effect of shear bands. Hays et al. [13] found that certain heterophases in an amorphous matrix could confine the propagation of shear bands and promote their multiplication. This multiplication can moderate the propagation of individual shear bands effectively, and thus, improve mechanical strength and ductility [6,13]. With this strategy, numerous reinforcements/amorphous matrix composites have been developed. Krishananand and Cahn [14] found that annealing below the glass transition temperature, which did not cause crystallization, could restore the ductility of a rolled amorphous alloy, and the recovered ductility is even somewhat greater than that of the as-formed alloy glass. However, the hardness was not observed to be affected by rolling or subsequent annealing. Interestingly, Pampillo [15] discovered that the susceptibility of shear

* Corresponding author. Tel.: +1 734 764 6888; fax: +1 734 763 4540.
E-mail address: atzmon@umich.edu (M. Atzmon).

1359-6454/$30.00
doi:10.1016/j.actamat.2005.04.003

bands in deformed, amorphous, Pd–Cu–Si to preferential etching could be eliminated by annealing. He assumed that the loss of chemical activity was caused by annealing-induced re-ordering within the shear bands. Research work on annealing of deformed amorphous alloys, a promising route for property recovery, has been rather limited.

Shear bands are usually identified and characterized morphologically by scanning electron microscopy (SEM) (see, e.g. [2,5]). However, less information is available on their nanoscale structure, as the relatively small changes in them are frequently undetectable by conventional transmission electron microscopy (TEM). Recently, Miller and Gibson [16] have developed a quantitative high-resolution TEM (HRTEM) method of characterizing the medium-range atomic structure of amorphous solids. This method includes quantitative analysis of electron images and their Fourier amplitudes, essentially combining small-angle scattering analysis and high-resolution imaging from the same microscopic region. This technique allowed the identification of nanometer-scale voids in amorphous silica thin films. Utilizing this technique, Li et al. [17] studied shear bands in bulk Zr-based metallic glasses and found that they contained a higher concentration of nanometer-scale voids than undeformed regions. Recently, we have investigated shear bands in the tensile and compressive regions in an amorphous Al-based alloy bent at room temperature, using quantitative HRTEM. We have found that the defect distribution in shear bands in the tensile region is substantially different from that in the compressive region, where mechanically induced nanocrystallization occurred [3]. Also, using this technique, we have been able to explain the presence or absence of deformation-induced nanocrystallites in similar alloys on the basis of the microstructure of the shear bands [18]. Thus, quantitative HRTEM is a potentially powerful tool for revealing defects in shear bands in deformed amorphous alloys.

Instrumented nanoindentation is an effective probe for studying the mechanical response of various materials to micro- and even nano-scale load. It makes it possible to detect nucleation of dislocations in crystalline materials [19,20]. This technique has also been applied widely to the study of plastic-deformation instability, i.e., serrated flow, of amorphous alloys, as recently reviewed by Schuh and Nieh [21]. Serration during nanoindentation is related to shear-band formation. Lately, combining instrumented nanoindentation with atomic force microscopy (AFM), we found that the loading rate affects shear-band formation, and consequently, the serrated flow of an amorphous alloy [9].

Mechanical properties of amorphous alloys at low temperatures and high strain rates are closely related to shear-band formation and propagation. Research work on this relationship is of fundamental interest and also of practical significance for processing and service of amorphous alloys, and therefore, has received much attention. However, to the authors' knowledge, to date, published work has been limited to the effect of the morphology of shear bands on mechanical properties, but the relationship between the structure of shear bands and their properties has not been addressed. In the present work, we explore the structure of shear bands in an amorphous Al–Ni–Y alloy that was rolled at room temperature, and subsequently annealed at elevated temperature, using quantitative HRTEM. The mechanical behavior is examined by nanoindentation and correlated with the structure. The amorphous Al–Ni–Y alloy selected for this work is immune to mechanically induced nanocrystallization [18,22], so that the change in structure and properties are attributable to the shear bands per se.

2. Experimental details

The material investigated in this study is amorphous $Al_{86.8}Ni_{3.7}Y_{9.5}$ (at.%). A ribbon, 22 μm thick and 1 mm wide, was obtained by the single-wheel melt-spinning technique using a Cr-coated Cu wheel at a tangential velocity of 40 m/s in vacuum. X-ray and electron diffraction analyses were employed to confirm the amorphous structure of the as-spun alloy ribbon. Samples were rolled in up to 100 small steps to a final thickness reduction of 45.5%. Some of the rolled samples were annealed at 110 °C for 60 min in a Ti-gettered, flowing-Ar, furnace.

Samples were prepared for nanoindentation tests by electropolishing from the wheel side of the ribbon, using a single-side jet thinning electropolisher. A solution of 25% nitric acid and 75% methanol was employed at 243 K and a voltage of 90 V. Load–displacement curves and hardness values were obtained from indentation experiments, performed using a Nanoinstruments Nanoindenter II with a Berkovich diamond indenter. At least 20 indents were made on each of multiple samples. The separation between adjacent indents was 20 μm. The loading phase of indentation was carried out under load control at a loading rate of 0.5 mN/s to a maximum load of 10 mN. At 90% unloading, a dwell period of 100 s was imposed to correct for any thermal drift in the system, which was less than 0.2 nm/s.

AFM observation on the indents was conducted using a Digital Instruments Nanoscope IIIa in contact mode. TEM specimens were prepared electrolytically by thinning from the wheel side of the ribbon, under the same condition as for nanoindentation (see above). The samples were investigated using a JEOL 2010F HRTEM at an operating voltage of 200 kV.

3. Results

3.1. Nanoindentation

Fig. 1(a) shows the loading portions of the load–displacement curves for the as-spun, rolled, rolled/annealed, and as-spun/annealed samples. The results for the as-spun and as-spun/annealed samples are included for comparison. From the nanoindentation data, the strain rates, $\dot{\varepsilon} = (1/h)(\mathrm{d}h/\mathrm{d}t)$, where h is the indenter displacement, during loading were calculated. The values change with depth, as shown in Fig. 1(b). The strain rates for all the samples show the same decreasing trend with increasing depth. However, the curves are not smooth and there is obvious serration above a certain depth. These curves highlight the serration behavior observed in the load–displacement curves (Fig. 1(a)). The as-spun sample exhibits obvious serrated flow. The rolled sample, on the other hand, reveals little serration, that is, rolling obviously moderates the serration. Annealing at 110 °C for 60 min substantially changes the flow behavior of the rolled sample, resulting in the recovery of serrated flow. It is also noted that the as-spun/annealed sample exhibits more pronounced serrated flow than the as-spun sample. The plastic-flow behavior of the amorphous alloy is obviously dependent on its thermo-mechanical history.

The hardness of the as-spun, rolled, rolled/annealed, and as-spun/annealed samples was derived from nanoindentation, as shown in Table 1. A correction was applied using the actual contact area of indents observed by AFM, in order to account for pile-up (see Section 4 below). It is important to mention that the hardness was obtained from nanoindentation with a maximum load of 10 mN and a loading rate of 0.5 mN/s. Due to an indentation-size effect, hardness values for amorphous alloys, derived from nanoindentation, are higher than those obtained from macro- or even microhardness testers [23,24]. Thus, the numbers we present are only used for comparison between our samples. Furthermore, our hardness values do not correspond to measurements at fixed depth. From the hardness-depth curves for as-spun, and rolled, amorphous Al-based alloys [25], we estimate that the difference in hardness resulting from the depth variations in the present work is less than about 1%, which is negligible. It can be seen that rolling significantly reduces the hardness. Subsequent annealing increases it to values higher than that for the as-spun sample, but still lower than that for the as-spun/annealed sample.

Table 1
Hardness (H) of Al–Ni–Y for different treatments

	As-spun	Rolled	Rolled/annealed	As-spun/annealed
H (GPa)	3.89 ± 0.03	3.48 ± 0.02	4.05 ± 0.04	4.35 ± 0.07

3.2. Morphological observation on indents

Extensive AFM observations on the indents in the as-spun, rolled, and rolled/annealed samples indicate that the indents were rather regular in shape and caused no cracking. Typical images are shown in Fig. 2. There are obvious pile-ups around the indents in the as-spun sample, with height of about 37% of the indent depth. However, very small pile-ups are observable around the indents in the rolled sample, and the height of the pile-ups is only 12% of the indent depth. Annealing between rolling and indenting causes the reappearance of pile-up behavior around the indents, with height of about 64% of the indent depth, which is even larger than that in the as-spun sample.

3.3. Structural observation on shear bands

3.3.1. TEM observation

TEM observation shows that numerous curved shear bands formed after severe rolling, indicating inhomogeneous plastic deformation (Fig. 3(a)). Selected-area

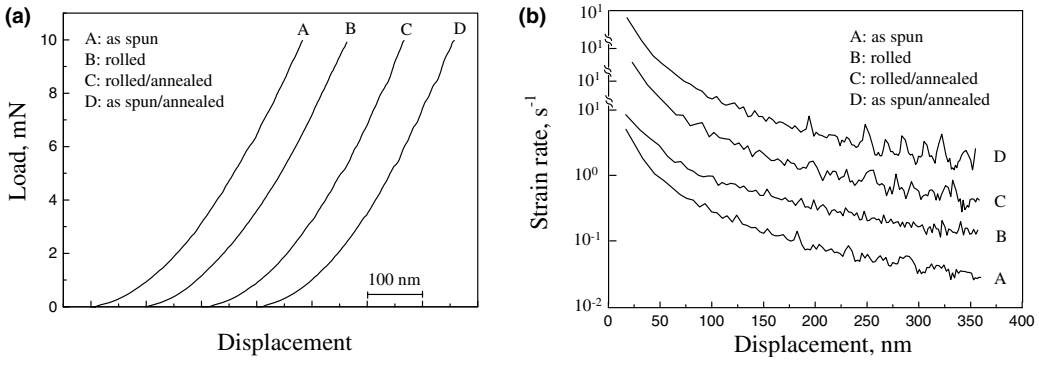

Fig. 1. (a) Loading portions of the load–displacement curves for the as-spun, rolled, rolled/annealed, and as-spun/annealed samples during nanoindentation. (b) Strain rate–displacement curves of the as-spun, rolled, rolled/annealed, and as-spun/annealed samples during loading under nanoindentation. In order to avoid overlapping, the curves (on a semi-log scale) of the rolled, rolled/annealed, and as-spun/annealed samples were shifted upward by $10^{0.5}$, $10^{1.2}$, and $10^{1.6}$ s^{-1}, respectively.

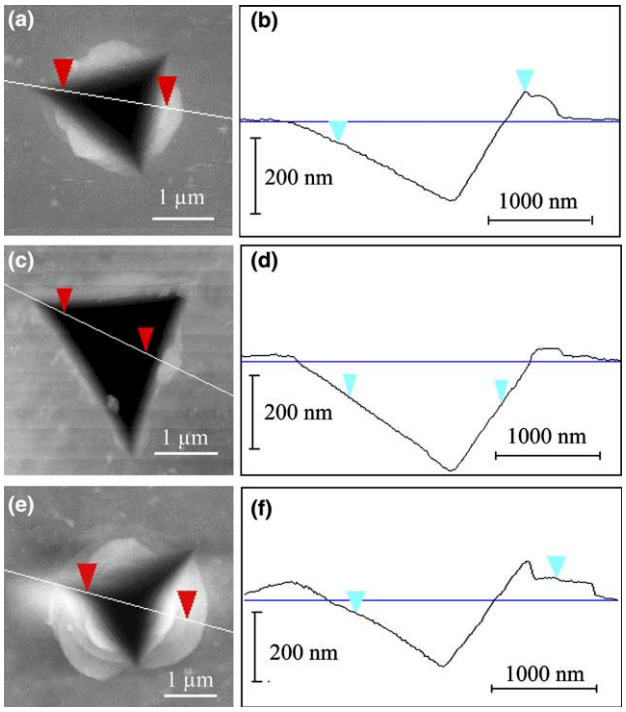

Fig. 2. AFM images and corresponding height profiles of indents formed at a maximum load of 10 mN in the as-spun sample (a, b), rolled sample (c, d), and rolled/annealed sample (e, f). The lines in the images indicate traces where height profiles were taken.

electron diffraction (SAED) demonstrates that no crystallization occurred in the sample. A typical electron diffraction pattern is shown in Fig. 3(b), which contains only diffuse rings from the amorphous matrix. Shear bands are still observable after annealing, as shown in Fig. 4(a). SAED reveals no crystallites in the rolled and annealed sample, and the sample is still amorphous (Fig. 4(b)). Dark-field images (not shown), obtained by placing the objective aperture on the diffuse ring corresponding to the amorphous matrix, did not exhibit any evidence for nanocrystallization in the rolled, annealed and rolled/annealed samples used in this study.

3.3.2. HRTEM observation

Following the method developed by Miller and Gibson [16] and later extended by Li et al. [17], the nanoscale structural characteristics of the shear bands in the rolled and rolled/annealed samples were investigated. Firstly, images at a defocus value of −200 nm were obtained. Their Fourier transforms were computed. We detected a prominent difference in the Fourier-transform amplitude between the shear band and undeformed region in the small-angle scattering region, similar to the result of Li et al. [17]. Similar results were obtained by Donovan and Stobbs [26], using axially aligned dark-field images for metallic glasses. In order to image the defects giving rise to the small-angle scattering, the Fourier transform was filtered by passing the spatial frequencies of interest ($0.5\ \mathrm{nm}^{-1} < k < 1.5\ \mathrm{nm}^{-1}$) and excluding all other spatial frequencies (see Li et al. [17]). A reverse Fourier transform was calculated to obtain a filtered image, which displays the projected atomic density. It does not contain contributions from the sample's thickness variation, since these have long wavelength, hence the uniform mesoscopically averaged intensity. Regions with locally lower (higher) density appear bright (dark) [17]. To identify density fluctuations which exceed those expected statistically, a threshold filter was then applied, set to display a signal only when the mean brightness is exceeded by three standard deviations. Finally, the images were inverted. Although the choice of the threshold filter is somewhat arbitrary and accurate quantification cannot be made, the results are of qualitative, even semi-quantitative, significance [16,17].

Fig. 5(a) is a HRTEM image of the rolled sample, containing both a part of a shear band and its neighboring, undeformed, matrix. The shear band appears bright and the undeformed matrix is dark, which is a result of thickness contrast: as they have less resistance to chemical attack during thinning, shear bands are thinned at a higher rate than the matrix [15]. It is noted that no nanocrystals formed in the undeformed matrix or the shear bands. Fig. 6(a) is an image filtered as described above. From Fig. 6(a), a threshold-filtered and inverted image was obtained (Fig. 7(a)). In it, the small spots indicate the location of low-density defects in Fig. 5(a). Obviously, there are more such defects, i.e., nanovoids [16,17], within the shear band than in the undeformed region. A similar image was obtained by Li et al. [17].

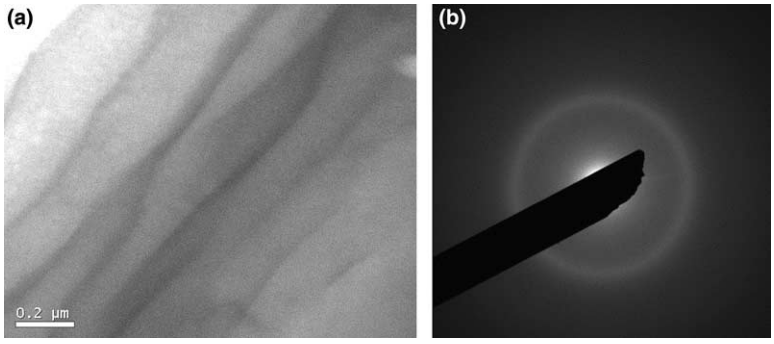

Fig. 3. TEM images of the rolled sample: (a) bright-field image; (b) SAED pattern.

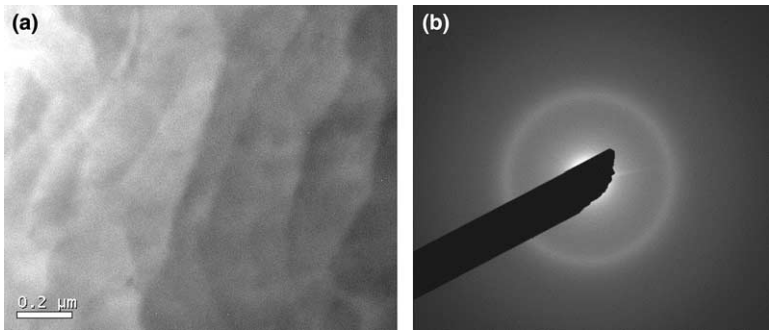

Fig. 4. TEM images of the rolled/annealed sample: (a) bright-field image; (b) SAED pattern.

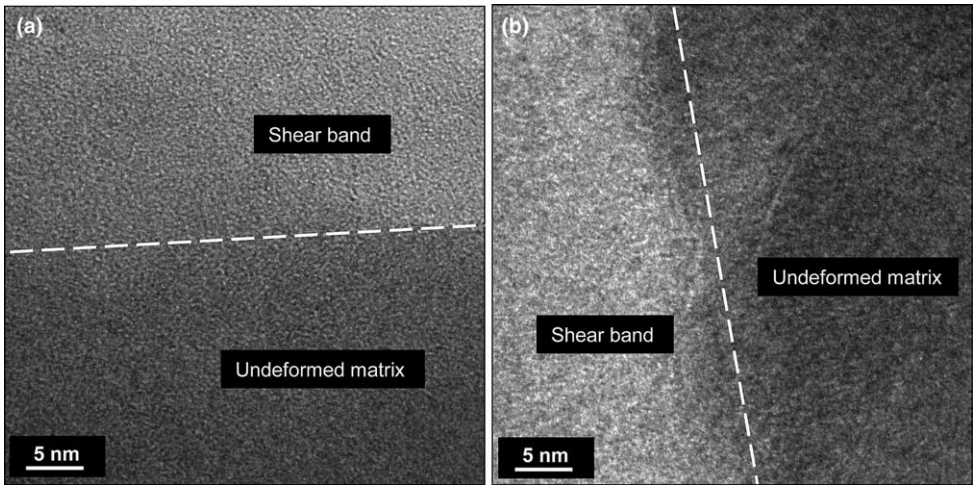

Fig. 5. HRTEM images showing a part of a shear band and its neighboring, undeformed, matrix in (a) the rolled sample, and (b) the rolled/annealed sample. The lines highlight the boundaries between the shear band and the undeformed matrix.

Fig. 5(b) is a HRTEM image of the rolled/annealed sample containing both a part of a shear band and its neighboring, undeformed, matrix. As in the rolled sample, the shear band is bright and the undeformed matrix dark, and no nanocrystals are observed. Using the same parameters as for the rolled sample, a frequency-filtered image (Fig. 6(b)) and a threshold-filtered, inverted, image (Fig. 7(b)) were obtained. This image seems to be similar to that for the rolled sample (Fig. 7(a)): the shear band contains more nanovoids than the undeformed matrix. This indicates that annealing did not significantly affect the nanovoids in the shear bands.

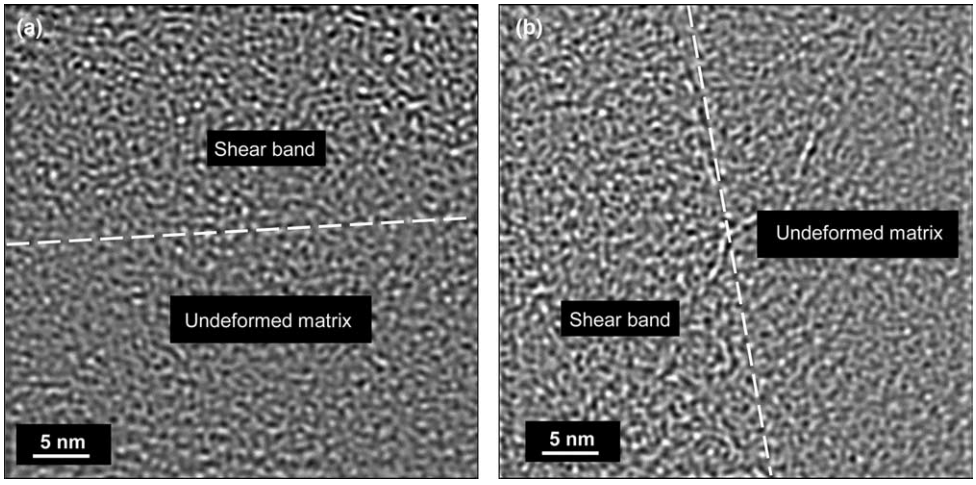

Fig. 6. Images at the same locations as Fig. 5, but defocused −200 nm, Fourier filtered.

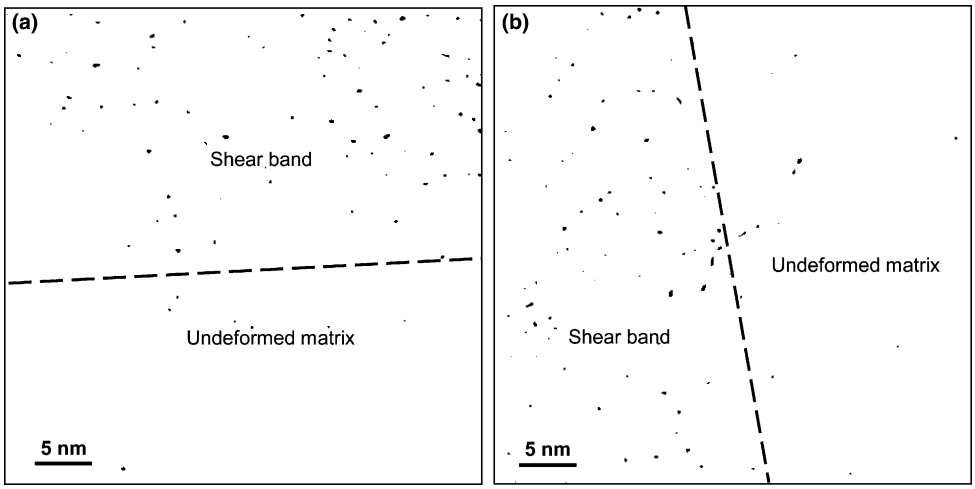

Fig. 7. Images at the same locations as Fig. 6, but threshold filtered and inverted.

Considering that nanovoids are observed mainly in the shear bands, which are thinner than the undeformed matrix, the imaging technique used reflects the structural details of the material rather than a thickness effect [17]. This comparison also lends support to the effectiveness of the method. Despite the fact that the images were processed in the same way, the imaging conditions for Fig. 7(a) and (b) were not identical, resulting in incomparability in the intensity. Therefore, it should be cautioned that a comparison of the absolute density of defects in the rolled sample with that in the rolled/annealed sample (Fig. 7(a) and (b)) is not possible. However, it is the comparison of variations within each sample that is significant.

4. Discussion

In the present work, heavy rolling led to the formation of numerous shear bands in amorphous $Al_{86.8}Ni_{3.7}Y_{9.5}$, and mechanically induced nanocrystallization did not occur (Fig. 4), in agreement with [18,22]. A rolling-induced change in structure and properties is assumed to be concentrated in the shear bands. Samples were rolled using multiple passes at a small amount of thickness reduction per pass, so as to minimize any thermal effect during deformation.

At low temperatures, serrated plastic flow of amorphous alloys is commonly observed in compression [27–31] and nanoindentation [9,10,32]. It has been attributed to the formation of discrete shear bands. Compared with compression tests on macroscopic samples, nanoindentation is sensitive to discontinuous flow, as it detects a deformation volume of nanometric dimensions. The critical strain rates, above which the serration could not be observed in a nanoindentation load–displacement curve, are about two orders of magnitude higher than those for compression of macroscopic specimens [32].

The as-spun sample exhibits obvious serrated plastic flow during nanoindentation. The authors believe this to be the first report on the reduction of the extent of serrations by rolling. Little serration in the rolled sample does not mean that homogeneous deformation occurred, which is expected at high temperatures and low strain rates. In the discussion below, we consider the fact that deformation can occur by nucleation and propagation of new shear bands or by propagation of those already present.

Pile-ups containing shear bands are commonly observed around indents in amorphous alloys [8,9,33,34]. However, the AFM results demonstrate that, compared with the as-spun sample, the rolled sample has very small pile-ups around indents. Using nanoindentation, Tang et al. [35] recently studied mechanical properties in the deformed zone around a large spherical indentation impression in a Zr-base metallic glass. Their AFM observation revealed smaller pile-ups around nanoindents close to the spherical indentation impression than far away. Vaidyanathan et al. [33] computationally predicted the location of the local maximum effective stresses to be along disconnected arcs surrounding the indent. Shear bands are expected to nucleate along these arcs, as confirmed by experiment. In the as-spun sample, obvious pile-ups around indents (Fig. 2(a)) indicate that during nanoindentation, inhomogeneous deformation occurred, and the deformation mechanism is the nucleation and propagation of new shear bands. New, concentric, shear bands form outside the indent as the indenter moves deeper into the sample, resulting in surface steps, as seen in Fig. 2(b). The nucleation of shear bands in an amorphous alloy results in serrations during plastic flow. Hufnagel et al. [2] observed that a serration in plastic flow in a three point bending test of a bulk amorphous alloy is due to the nucleation of a shear band. In the rolled sample, small pile-ups around the indents indicate that few new shear bands were generated

during nanoindentation, and the predominant deformation mechanism is therefore concluded to be the propagation of pre-existing shear bands, developed during rolling.

The presence of a great number of shear bands beneath indents in amorphous alloys was observed in experiment and simulation [36,37]. We note that during tensile deformation of an amorphous alloy sample, very few shear bands can form, and fracture occurs due to excessive propagation of few, or even a single shear band [11,12]. The reason for the formation of numerous shear bands in some deformation modes, such as compression, rolling, bending, etc., is due to geometric constraints. It is the extensive formation of shear bands that makes an amorphous alloy exhibit a substantial amount of ductility. Since the deformation mechanism in the rolled sample is the propagation of preexisting shear bands, the hardness of the rolled sample is substantially affected by the intrinsic mechanical strength of shear bands that were developed during rolling. Preexisting shear bands are the weak links in deformed, amorphous, alloys, as evidenced by the direct observation that they are preferential sites for subsequent deformation [14,30,38]. Deformation softening of an amorphous alloy has been widely observed, e.g. [35,39–41].

At the low annealing temperature used, the alloy retained its amorphous structure. However, significant relaxation took place in the shear bands. The rolled/annealed sample exhibits significant serrations, even more pronounced than the as-spun sample. This indicates that annealing is effective in causing relaxation of the shear bands developed during rolling, so that they are no longer the weak link. Therefore, the deformation mechanism based on nucleation and propagation of new shear bands is recovered. This is confirmed by the existence of substantial pile-ups with surface steps around the indents (Fig. 2(c)). Annealing increases the hardness noticeably, which is even higher than that of the as-spun sample. Evidently, this may be attributed to both the recovery of shear bands and the relaxation of the undeformed matrix, which make the amorphous alloy stronger (see Table 1). We note that the annealed, undeformed sample has the highest hardness. We attribute this hardening of the as-spun sample by annealing to free-volume relaxation.

Shear bands have a more disordered structure than the undeformed matrix, as short-range order, both chemical and topological, is destroyed by deformation [15,38,42,43]. This creates a chemical–potential difference between the shear bands and the undeformed matrix and consequently, the former is more susceptible to both chemical and/or electrochemical etching [30,38]. That is the reason that shear bands are observable in an electrolytically thinned sample (Fig. 3). Annealing may alleviate the susceptibility of shear bands to etching, and even eliminated their preferential etching. Such an effect of annealing was attributed to the recovery of short-range order in shear bands [38]. In our annealed sample, shear bands are still observable, albeit not as distinctly as before annealing (Fig. 4). We suggest that structural relaxation requires diffusion distances that are less than an atomic diameter, whereas re-establishment of chemical order requires greater diffusion length, not achieved under the present annealing conditions.

The direct observation of defects in amorphous alloys is significantly more challenging than in crystalline alloys. Using a recently developed quantitative HRTEM technique, the present work clearly reveals defects and their distribution. The shear bands contain more nanovoids than the undeformed matrix. TEM observation shows that annealing did not eliminate shear bands developed during rolling, and they are still observable (Fig. 4(a)). Quantitative HRTEM demonstrates no substantial difference in structure between shear bands in the rolled sample and those in the rolled/annealed sample (Fig. 7(a) and (b)). Although the technique does not allow a quantitative comparison of the nanovoid populations in various samples, we can obtain information on their distribution in the individual samples. In the rolled sample, the interior of the shear bands contains a higher density of nanovoids than the surrounding undeformed region (Fig. 7(a)). Annealing did not modify the distribution of nanovoids in shear bands, and the interior of the shear bands still contains numerous nanovoids (Fig. 7(b)).

Free-volume models for the kinetics of plastic flow in amorphous alloys have predicted the creation of excess free volume in shear bands during plastic deformation [44–46]. Lately, using real-time diffraction with synchrotron radiation, Hajlaoui et al. [34] obtained evidence of free volume generation due to plastic deformation in Zr-based amorphous alloys – more than 37% average additional free volume created by cold plastic deformation, as compared to the as-quenched state. Their conclusion was based on the assumption that the magnitude of the wave vector at which the diffraction pattern has a maximum is proportional to the cubic root of the number density. Using positron annihilation spectroscopy, Flores et al. [47] also demonstrated that plastic deformation increased the amount of free volume in a bulk Zr-based amorphous alloy. Donovan and Stobbs [26], in their model of shear bands, argued that a shear band is dilated even when under compression. Wright et al. [48] and Li et al. [49] proposed that the formation of nanovoids in shear bands is a thermodynamically favorable process. This would indicate that shear bands with excess free volume are thermodynamically unstable. As soon as the applied stress is removed, excess free volume tends to decrease by escaping from the shear bands and/or condensing into voids. However, after

the applied stress is removed, shear bands still contain frozen excess free volume, as the atomic mobility in shear bands is limited at low temperatures. Relaxation at elevated temperatures, below the glass transition temperature, results in a decrease in free volume in amorphous alloys [34,47,50]. Consequently, the number of voids in a shear band might increase. However, such a determination cannot be made based on our data.

Rolling results in a decrease in hardness of the amorphous alloy, i.e., deformation softening (Table 1). This is consistent with the theoretical treatment of [44,45]. Tang et al. [35] also detected a lower hardness in the deformed zone around a large spherical indentation impression in a Zr-based amorphous alloy. Regions with high free volume are expected to have a lower strength [45]. The lower hardness of the rolled sample may be attributed to the excess free volume remaining in shear bands after nanovoid formation. As mentioned previously, annealing may recover the structure of shear bands through reordering [38] and reduction of the excess free volume [34,46,48]. In the present work, the recovery by annealing is incomplete, as shear bands are still preferentially etched. However, the deformation mechanism was substantially recovered, as evidenced by the formation of pile-ups containing shear bands around the indents (Fig. 2(e) and (f)). This recovery of the plastic-deformation resistance of the shear bands must have resulted from removal of excess free volume in them. The incomplete recovery, evidenced by the persistence of preferential etching, may be due to incomplete recovery in chemical order [30]. Furthermore, it can be deduced that chemical order has less effect on strength than the free volume does. The increase in hardness, and recovery of serrated flow by annealing, is attributed to a decrease in excess free volume. From the fact that the rolled/annealed sample has a distribution of nanovoids similar to that in the rolled sample and hardness higher than that of the rolled sample, and even higher than that of the as-spun sample, we can conclude that the excess free volume has a more substantial impact on plastic-deformation resistance of shear bands than the nanovoids in them. However, the nanovoids possibly contribute to the lower hardness of the rolled/annealed sample as compared to that of the as-spun/annealed sample.

5. Conclusions

Using nanoindentation, AFM and HRTEM, the effect of room-temperature rolling to a thickness reduction of 45.5%, and subsequent annealing (110 °C/60 min), on the mechanical behavior and microstructure of amorphous $Al_{86.8}Ni_{3.7}Y_{9.5}$ was investigated. The main results can be summarized as follows:

1. Rolling reduces the amplitude of serrations in the load–displacement curve, compared to that of the as-spun amorphous alloy. The predominant deformation mechanism in the rolled sample is the propagation of pre-existing shear bands. Rolling results in deformation softening.
2. Annealing can effectively relax the shear bands and undeformed matrix in the rolled sample. It leads to a recovery of serrated flow. The rolled/annealed sample exhibits even more pronounced serrations than the as-spun sample. Also, annealing increases the hardness of the rolled sample substantially. As in the as-spun sample, the predominant deformation mechanism in the rolled/annealed sample is nucleation and propagation of new shear bands. Although chemical disorder appears to be retained in the shear bands after annealing, it does not have a strong effect on the mechanical behavior.
3. Combining HRTEM with Fourier transform filtering, defects, i.e., nanovoids, in the shear bands in the rolled, and rolled/annealed samples were imaged. In the rolled sample, a great number of nanovoids are located in the interior of shear bands. Annealing does not change the distribution of defects in shear bands significantly.
4. Nanovoids retained after relaxation annealing might be detrimental to mechanical strength. However, the excess free volume has a more significant impact on plastic-deformation resistance of shear bands than do the nanovoids.

Acknowledgments

This work was funded by the U.S. National Science Foundation, Grant DMR-0314214. The JEOL-2010F HRTEM used in this work was funded by NSF through the Grant DMR-9871177 and is operated by the Electron Microbeam Analysis Laboratory at the University of Michigan, Ann Arbor, MI.

References

[1] Takayama S, Maddin R. Acta Metall 1975;23:943.
[2] Hufnagel TC, El-Deiry P, Vinci RP. Scripta Mater 2000;43:1071.
[3] Jiang WH, Atzmon M. Acta Mater 2003;51:4095.
[4] Jiang WH, Pinkerton FE, Atzmon M. Scripta Mater 2003;48:1195.
[5] Conner RD, Johnson WL, Paton NE, Nix WD. J Appl Phys 2003;94:904.
[6] Bian Z, He G, Chen GL. Scripta Mater 2002;46:407.
[7] Pekarskaya E, Kim CP, Johnson WL. J Mater Res 2001;16:2513.
[8] Kim JJ, Choi Y, Suresh S, Argon AS. Science 2002;295:654.
[9] Jiang WH, Atzmon M. J Mater Res 2003;18:755.
[10] Greer AL, Castellero A, Madge SV, Walker IT, Wilde JR. Mater Sci Eng A 2004;375–377:1182.

[11] Mukai T, Nieh TG, Kawamura Y, Inoue A, Higashi K. Scripta Mater 2002;46:43.
[12] Zhang ZF, Eckert J, Schultz L. Acta Mater 2003;51:1167.
[13] Hays CC, Kim CP, Johnson WL. Phys Rev Lett 2000;84:2901.
[14] Krishananand KD, Cahn RW. Scripta Metall 1975;9:1259.
[15] Pampillo CA. Scripta Metall 1972;6:915.
[16] Miller PD, Gibson MJ. Ultramicroscopy 1998;74:221.
[17] Li J, Wang ZL, Hufnagel TC. Phys Rev B 2002;65:144201.
[18] Jiang WH, Pinkerton FE, Atzmon M. J Mater Res 2005;20:696.
[19] Gerberich WW, Nelson JC, Lilleodden ET, Anderson P, Wyrobek JT. Acta Mater 1996;44:3585.
[20] Gouldstone A, Koh HJ, Zeng KY, Giannakopoulos AE, Suresh S. Acta Mater 2000;48:2277.
[21] Schuh CA, Nieh TG. J Mater Res 2004;19:46.
[22] He Y, Shiflet GJ, Poon SJ. Acta Metall Mater 1995;43:83.
[23] Lam DCC, Chong ACM. Mater Sci Eng A 2001;318:313.
[24] Mayo MJ, Siegel RW, Narayanasami A, Nix WD. J Mater Res 1990;5:1073.
[25] Jiang WH, Atzmon M. Appl Phys Lett 2005;86:151916.
[26] Donovan PE, Stobbs WM. Acta Metall 1981;29:1419.
[27] Wright WJ, Saha R, Nix WD. Mater Trans JIM 2001;42:642.
[28] Wright WJ, Schwarz RB, Nix WD. Mater Sci Eng A 2001;319–321:229.
[29] Kimura H, Masumoto T. Acta Metall 1983;31:231.
[30] Pampillo CA, Chen HS. Mater Sci Eng 1974;13:181.
[31] Donovan PE. Acta Metall 1989;37:445.
[32] Schuh CA, Nieh TG. J Mater Res 2002;17:1651.
[33] Vaidyanathan R, Dao M, Ravichandran G, Suresh S. Acta Mater 2001;49:3781.
[34] Hajlaoui K, Benameur T, Vaughan G, Yavari AR. Scripta Mater 2004;51:843.
[35] Tang CG, Li Y, Zeng KY. Mater Sci Eng A 2004;384:215.
[36] Jana S, Ramamurty U, Chattopadhyay K, Kawamura Y. Mater Sci Eng A 2004;1191:375.
[37] Shi YF, Falk ML. Appl Phys Lett 2005;86:011914.
[38] Vianco PT, Li JCM. J Mater Sci 1987;22:3129.
[39] Chen HS. Scripta Metall 1975;9:411.
[40] Sergueeva AV, Mara N, Mukherjee AK. J Non-cryst Solids 2003;317:169.
[41] Masumoto T, Maddin R. Mater Sci Eng 1975;19:1.
[42] Guoan W, Cowlam N, Gibbs MRJ. J Mater Sci 1984;19:1374.
[43] Polk DE, Turnbull D. Acta Metall 1972;20:493.
[44] Spaepen F. Acta Metall 1977;25:407.
[45] Argon AS. Acta Metall 1979;27:47.
[46] Steif PS, Spaepen F, Hutchinson JW. Acta Metall 1982;30:447.
[47] Flores KM, Suh D, Dauskardt RH. J Mater Res 2002;17:1153.
[48] Wright WJ, Hufnagel TC, Nix WD. J Appl Phys 2003;93:1432.
[49] Li J, Spaepen F, Hufnagel TC. Philos Mag A 2002;82:2630.
[50] Suh D, Dauskardt RH. J Non-cryst Solids 2003;317:181.